JOURNAL OF SOLID STATE CHEMISTRY 112, 1–8 (1994)

Thermal Evolution of the Crystal Structure of the Rhombohedral $Bi_{0.75}Sr_{0.25}O_{1.375}$ Phase: A Single Crystal Neutron Diffraction Study

D. Mercurio, J. C. Champarnaud-Mesjard, and B. Frit[1]

Laboratoire de Matériaux Céramiques et Traitements de Surface, U.R.A.-C.N.R.S. no. 320, Faculté des Sciences de Limoges, 123, Avenue Albert-Thomas, 87060 Limoges Cedex, France

P. Conflant and J. C. Boivin

Equipe de Cristallochimie et Physicochimie du Solide, U.R.A.-C.N.R.S. no. 452, E.N.S.C.L., Université de Lille I, B.P. 108, 59652 Villeneuve d'Ascq Cedex, France

and

T. Vogt[2]

Physics Department, Brookhaven National Laboratory, Upton, Long Island, New York 11973

Received June 7, 1993; in revised form October 11, 1993; accepted October 21, 1993

The crystal structure of the rhombohedral ($R\bar{3}m$) $Bi_{0.75}Sr_{0.25}O_{1.375}$ phase has been determined at room and high temperature using single crystal neutron diffraction. It can be described at all temperatures as the regular repetition of three fluorite-like sheets shifted with respect to one another by a vector μ = 2 (a/3 + b/3 + c/3) and thus separated by an intersheet space free of anions. Interstitial anions partially occupy delocalized sites in the vicinity of the unsubstituted interface Bi-layers and are responsible for the high ionic conductivity of this phase. They are mainly located on the fluorite-like sheet side of this Bi-layer at room temperature. At high temperature, they partly migrate to the opposite side, i.e., the intersheet side, a phenomenon which results in the $\beta_2 \Rightarrow \beta_1$ transition and a sudden increase of the conductivity. In light of these and previous results the different behavior of various alkaline earth-doped rhombohedral phases (Ca, Sr, Ba) and of the La-doped homologue is analyzed and rationalized.

I. INTRODUCTION

Doping of Bi_2O_3 with various different oxides results in numerous nonstoichiometric anion-deficient fluorite-related phases which very often reveal high ionic conductivity. One of them with a rhombohedral symmetry has been isolated within the Bi_2O_3–MO (M = Ca, Sr, Ba) (1–5), Bi_2O_3–Ln_2O_3 (Ln = La, Sm, Gd) (6, 7), Bi_2O_3–Ln_2O_3–TeO_2 (Ln = La, Sm, Gd, Er) (8), Bi_2O_3–CdF_2, Bi_2O_3–La_2O_3–MF_2 (M = Cd, Pb), and Bi_2O_3–CdF_2–PbF_2 (9) systems. For each system, this phase undergoes a reversible polymorphic phase transition ($\beta_2 \Leftrightarrow \beta_1$) which results generally in a sudden increase of the conductivity (10–12).

Since the pioneering powder X-ray investigations of Sillen and Aurivillius (1, 2), the crystal structure of the β_2 polymorph at room temperature has been the subject of numerous studies either by single crystal X-ray diffraction (5, 10, 12, 14, 16) or by powder neutron diffraction (15, 16) techniques. As shown in Fig. 1, the structure consists of a regular repetition along the c-axis of 3^6 hexagonal close packed metal layers with the sequence ABC–BCA–CAB, i.e., *chh chh chh*, and with alkaline earth or rare earth cations located on every third hexagonal layer ($M(1)$ sites). The tetrahedral sites of this packing are occupied with oxygen atoms O(1) and O(2) (for the ccp part) and by a lone pair (E) of bismuth atoms (for the hcp part). Such a structure can therefore be described as a regular repetition along the c-axis of identical fluorite-like sheets. Each sheet is built up of three hexagonal metal layers (one internal layer of Bi/alkaline earth or rare earth metal in distorted cubic eightfold coordination, surrounded by two external layers of Bi atoms in dissymmetrical fourfold coordination: BiO_4 E) and accommodates the majority of the anions (i.e., oxygen atoms O(1) and O(2)) in its tetrahedral sites. Extra anions partially occupy delocalized "interstitial" sites within the vacant octahe-

[1] To whom correspondence should be addressed.

[2] On leave from Institut Laue-Langevin, 156X, 38042 Grenoble cedex, France.

0022-4596/94 $6.00

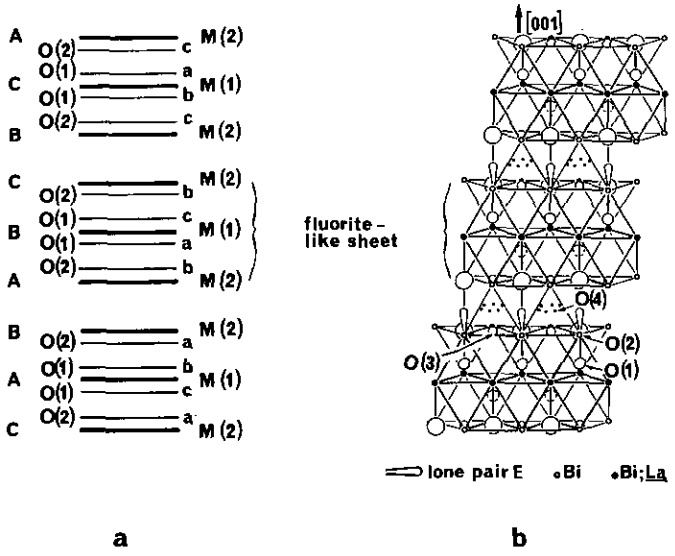

FIG. 1. The $Bi_{0.7}La_{0.30}O_{1.5}$ crystal structure (16). (a) Sequence along the c-axis of hexagonal 3^6 cationic (A, B, C) and anionic (a, b, c) layers. (b) Location of the different anions within the cationic polyhedral network.

dra of the intersheet space: O(3) sites near the basal triangular face of the octahedra, and only in the case of the $Bi_{0.70}La_{0.30}O_{1.50}$ phase, O(4) sites near the center of the octahedra. We must point out that, in order to avoid O(1)–O(2) distances which are too short within the fluorite-like sheets and aided by a very low anionic density within the intersheet space, the O(2) atoms are shifted from the ideal tetrahedral sites (always partly occupied) toward the triangular face of the metal layer interface.

As the β_1 polymorph is impossible to stabilize as a metastable state at room temperature, up to now only high-temperature single crystal X-ray diffraction experiments have been performed (5, 10). If they confirm what the thermal evolution of the powder patterns suggests, i.e., a great structural analogy with the β_2 form, they do not unambiguously allow for the determination of the number and the locations of interstitial anions within the intersheet space. So, in order to (i) accurately locate, both at room and higher temperatures, the interstitial anions in a rhombohedral phase less rich in anions than the $Bi_{0.70}Sr_{0.30}O_{1.50}$ phase, and (ii) clearly determine the structural features of the $\beta_2 \Leftrightarrow \beta_1$ transition, whose impact on the electrical properties is far more important with the alkaline earth-doped phases (see Fig. 8), we decided to undertake a single crystal neutron diffraction study, at temperatures below and above the transition temperature, of the $Bi_{0.75}Sr_{0.25}O_{1.375}$ phase.

II. EXPERIMENTAL

Single crystals were prepared by melting at 1270 K in a platinum crucible, and then slowly cooling down (2 K/hr). From the numerous laminar and frequently foliated $Bi_{0.75}Sr_{0.25}O_{1.375}$ crystals, one with a suitable form, size ($4 \times 0.5 \times 0.1$ mm^3), and quality was selected.

Bragg intensities were collected at the Institut Laue-Langevin, France on the D19 diffractomer using a wavelength of 1.043 Å. D19 is a four-circle diffractometer equipped with a vertically curved two-dimensional position-sensitive detector (17). The 2D-PSD is built up of 16 cathode and 512 anode wires and situated 1.15 m from the sample, covering a solid angle of 4° horizontally and 64° vertically. The detector is filled with ^{3}He gas at 6 atm pressure and argon at 1 atm as quenching gas.

Measurements were performed at three different temperatures: 300 and 600 K for the β_2-phase and 1050 K for the β_1 polymorph (transition temperature 930 K).

Using a 2D-PSD a single ω-scan yields information about three directions in reciprocal space rather than one obtained with a single detector. This allows for an easy detection of powder lines and other parasitic scattering due to sample environments, e.g., furnace shields. Also, very weak reflections are measured more reliably since the background is much more well defined.

The integrated intensities were extracted as described by Wilkinson and Khamis (18). Because of the change of the unit cell parameters the orientation matrix was determined at each temperature. In each case 118 independent reflections satisfying the $I > 3\sigma(I)$ criterion were retained. All the refinement calculations were performed using the SHELX76 (19) and the scattering lengths (Fm): $b_{Bi} = 8.53$, $b_{Sr} = 7.05$, $b_O = 5.805$.

III. DETERMINATION OF THE STRUCTURE

The refinements were done using the centrosymmetrical space group $R\bar{3}m$ and following strictly the same procedure for the three data sets. Our starting model was the one obtained by Conflant *et al.* (3) for $Bi_{0.765}Sr_{0.235}O_{1.383}$

–2.25 Sr and 0.75 Bi on the $M(1)$ site (3a: 0, 0, 0)
–6 Bi on the $M(2)$ site (6c: 0, 0, 0.22)
–6 O on the O(1) site (6c: 0, 0, 0.29)
–6 O on the O(2) site (6c: 0, 0, 0.10)

The isotropic thermal coefficients of the cations and anions were fixed at reasonable values, 0.5 and 1.5 Å^2, respectively. The refinements converged quite well, indicating that, as for all previously studied phases, the O(2) site was partly occupied.

Using this model, difference Fourier syntheses were then performed. They revealed the presence of three extra partly occupied anionic sites: the O(3) site (6c: 0, 0, 0.44), similar to that observed for the $Bi_{0.7}La_{0.3}O_{1.5}$ phase; two extra sites O(2)′ and O(3)′ in 18 h position, (x, $2x$, z) which correspond to a splitting of, respectively, the O(2) and O(3) sites. The latter is observed only for the β_1 polymorph (see Fig. 2).

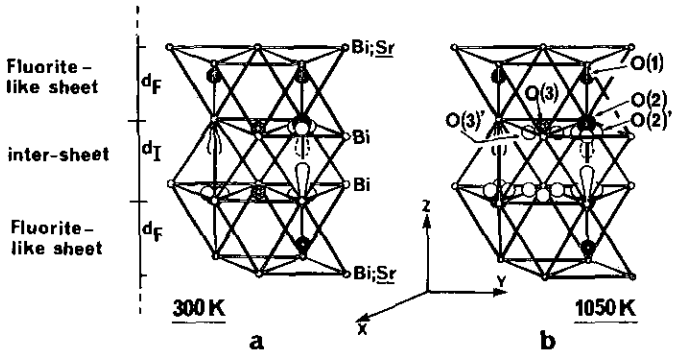

FIG. 2. Visualization of the "interstitial" anions O(3), O(3)', and O(2)' in the vicinity of the external Bi-layers of the fluorite-like sheets at 300 K (a) and 1050 K (b).

Due to the high correlations observed between the occupancy and the thermal parameters of these two sites, they were never simultaneously refined. In the last steps of the refinement the anisotropic displacement parameters of the cations and the O(1) and O(2) anions were introduced. The final parameters are listed in Table 1 and the main interatomic distances are given in Table 2. One can see that the refined occupancies lead to a total number of anions per unit cell which is in good agreement with the theoretical number 12.375.

IV. RESULTS AND DISCUSSION

1. Structure at Room Temperature (β_2-form). Comparison with the $Bi_{0.70}La_{0.30}O_{1.50}$ Homologue

Our results, illustrated by the schematic view in Fig. 2a and the values of Table 2, confirm and complete the previous results of Conflant *et al.* (5, 14) and Blower and Greaves (15), i.e.,

- the cationic distribution among the $M(1)$ and $M(2)$ sites;
- the partial occupancy of the O(2) site within the fluorite-like sheets, and its displacement toward the intersheet space;
- the delocalization of the "interstitial" anions, and their absence from the intersheet ideal octahedral site (only really available since the tetrahedral sites are (i) already occupied by the Bi lone pair E and (ii) very close to the O(2) anions) since they are essentially located in the vicinity of the unsubstituted Bi-layers, either on the fluorite-like sheet side (O(2)' anions) or on the intersheet side (O(3) anions) (see Figs. 2 and 5).

The absence of the interstitial anions from the intersheet space distinguishes the alkaline earth-doped β_2-phases from their La-doped homologues. In these latter phases some interstitial anions are actually present on octahedral intersheets sites (O(4) sites on Fig. 1).

Due to the existence of bonding interactions between these extra O(4) anions and the Bi-atoms of the interface $M(2)$ layers, a flattening of the intersheet space occurs (see the abnormally low value of d_I with respect to d_F for the $Bi_{0.7}La_{0.3}O_{1.5}$ phase, among the series of values reported in Fig. 3b) and accounts for the abnormally high and low unit cell parameters (Fig. 3a). We will return later to the influence of such differences on the anionic diffusion processes and therefore on the electrical properties of these phases.

TABLE 1
Refined Parameters at Three Temperatures for the $Bi_{0.75}Sr_{0.25}O_{1.375}$ Phase

		β_2		β_1
Atom/site	Parameters	300 K	600 K	1050 K
$M(1)$	B_{eq} (Å^2)	1.67	2.23	3.38
$3a$ (0, 0, 0)	n_{Sr}	2.25	2.25	2.25
	n_{Bi}	0.75	0.75	0.75
$M(2)$	z	0.2244(1)	0.2246(1)	0.2250(1)
$6c$ (0, 0, z)	B_{eq} (Å^2)	1.31	1.95	3.11
	n_{Bi}	6	6	6
O(1)	z	0.2949(2)	0.2948(2)	0.2950(2)
$6c$ (0, 0, z)	B_{eq} (Å^2)	2.20	3.19	4.63
	n	6	6	6
O(2)	z	0.0981(7)	0.0992(15)	0.0968(14)
$6c$ (0, 0, z)	B_{eq} (Å^2)	2.48	2.97	3.97
	n	1.0(1)	1.1(1)	0.7(2)
O(2)'	x	0.0551(18)	0.0711(58)	0.0682(69)
$18h$ (x, $2x$, z)	z	0.1033(4)	0.1050(10)	0.1131(11)
	B_{iso} (Å^2)	2.48(88)	3.17(50)	3.44(37)
	n	3.9(2)	2.9(2)	2.8(3)
O(3)	z	0.448(8)	0.4468(8)	0.4437(12)
$6c$ (0, 0, z)	B_{iso} (Å^2)	1.91(56)	3.69(50)	5.11(1.17)
	n	1.3(2)	2.2(2)	2.1(3)
O(3)'	x			0.2260(99)
$18h$ (x, $2x$, z)	z			0.1177(11)
	B_{iso} (Å^2)			4.56(1.37)
	n			0.7(5)
	Σ_{n_O}	12.2	12.2	12.3
	a (Å)	3.970	3.983	4.011
	c (Å)	28.54	28.69	29.01
	V (Å^3)	389.55	394.17	404.19
	R_w	2.42	3.85	4.30

Anisotropic thermal coefficients ($\times 10^4$ Å^2)

Atoms	Temp. (K)	$U_{11} = U_{22}$	U_{33}	U_{12}
	300	139(15)	429(5)	70(13)
$M(1)$	600	224(19)	511(34)	112(10)
	1050	384(17)	710(36)	192(9)
	300	239(11)	139(33)	119(6)
$M(2)$	600	325(13)	254(19)	163(7)
	1050	527(13)	390(16)	263(7)
	300	456(20)	152(57)	228(10)
O(1)	600	756(142)	287(33)	586(211)
	1050	829(25)	515(34)	414(12)
	300	380(78)	371(78)	190(39)
O(2)	600	508(118)	473(208)	353(482)
	1050	860(150)	218(147)	430(75)

TABLE 2
Main Interatomic Distances and Structural Characteristics at Three Temperatures for the $Bi_{0.75}Sr_{0.25}O_{1.375}$

	β_2		β_1
Distances (Å)	300 K	600 K	1050 K
$M(1)$–$M(2)$	3.8625(9)	3.8801(9)	3.9033(9)
$(M(2)$–$M(2))_F = a$	3.970(2)	3.983(2)	4.011(2)
$(M(2)$–$M(2))_I$	4.0142(2)	4.0327(9)	4.1006(2)
$M(1)$–O(1)	2.541(2)	2.550(2)	2.568(2)
$M(1)$–O(2)	2.800(6)	2.814(14)	2.866(14)
$M(1)$–O(2)′	2.972(51)	2.988(32)	3.315(33)
$M(2)$–O(1)	2.012(2)	2.023(21)	2.031(2)
$M(2)$–O(2)	2.313(6)	2.320(14)	2.331(14)
$M(2)$–O(2)′	2.134(51)	2.141(11)	2.123(33)
	2.676(51)	2.684(11)	2.792(33)
	3.477(51)	3.495(11)	3.280(33)
$M(2)$–O(3)	2.296(7)	2.305(7)	2.316(11)
$M(2)$–O(3)′			2.065(23)
			3.072(123)
			3.486(123)
O(1)–O(1)	3.173(4)	3.186(4)	3.210(4)
O(1)–O(2)	2.855(34)	2.867(14)	2.905(14)
O(1)–O(2)′	2.821(51)	2.832(11)	3.032(33)
	3.250(51)	3.262(11)	3.533(33)
O(1)–O(3)	3.162(8)	3.175(8)	3.119(11)
O(2)–O(2)′	3.650(51)	3.662(17)	3.631(36)
	3.991(51)	4.004(17)	4.059(36)
O(2)–O(3)	2.341(10)	2.349(16)	2.339(18)
O(2)′–O(2)′	3.314(102)	3.325(21)	3.189(66)
	3.686(102)	4.004(21)	3.669(66)
O(2)′–O(3)	2.524(51)	2.533(13)	2.586(35)
	3.806(51)	3.824(13)	3.681(35)
O(2)′–O(3)′			2.309(127)
			2.937(127)
			2.310(127)
			3.379(127)
			3.836(127)
			3.695(127)
O(3)–O(3)	2.962(15)	2.978(15)	3.267(23)
O(3)–O(3)′			3.392(124)
			3.266(124)
			3.143(124)
O(3)′–O(3)′			2.719(247)
			3.545(247)
d_F	3.108	3.119	3.142
d_I	3.294	3.323	3.383
R_{F-F}	2.251	2.259	2.274
R_{F-I}	2.292	2.299	2.315
R_{I-I}	2.309	2.319	2.351
$d_{W-O(1)}$	2.245	2.245	2.267

Note. d_F and d_I are the thickness of respectively half the fluorite-like sheets and the intersheet space. R_{F-I} is the radius of the horizontal windows at the interface. R_{F-F} and R_{I-I} are the radii of the lateral windows within, respectively, the fluorite-like sheets and the intersheet space. $d_{W-O(1)}$ is the distance from an O(1) anion to the center of the lateral F–F window.

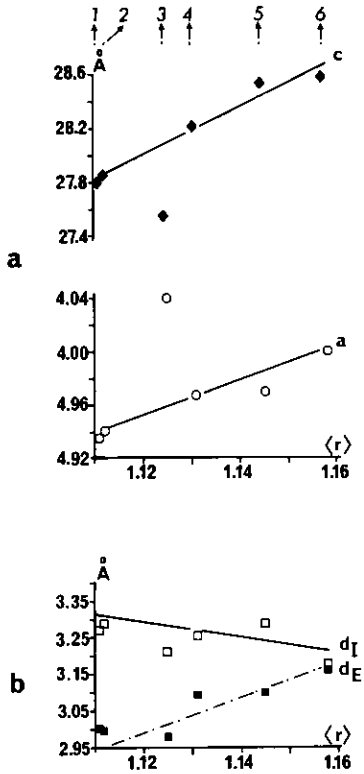

FIG. 3. Evolution with the mean cationic radius (calculated on the basis of Shannon–Prewitt values (20)) of (a) the unit cell parameters and (b) the half height d_F and the height d_I of respectively the fluorite-like sheet and the intersheet space for various rhombohedral phases at room temperature. (1) $Ca_{0.156}Bi_{0.844}O_{1.422}$ (5); (2) $Ca_{0.176}Bi_{0.824}O_{1.412}$ (15); (3) $La_{0.30}Bi_{0.70}O_{1.50}$ (16); (4) $Sr_{0.156}Bi_{0.844}O_{1.422}$ (5); (5) $Sr_{0.25}Bi_{0.75}O_{1.375}$ (this work); (6) $Ba_{0.156}Bi_{0.844}O_{1.422}$ (5).

2. *Thermal Evolution: The $\beta_2 \Leftrightarrow \beta_1$ Transition*

Figure 4 shows the thermal evolution of the powder X-ray diffraction pattern of the $Bi_{0.75}Sr_{0.25}O_{1.375}$ phase. We can see that the $\beta_2 \Leftrightarrow \beta_1$ transition simply leads to a sudden increase of the unit cell parameters without any significant

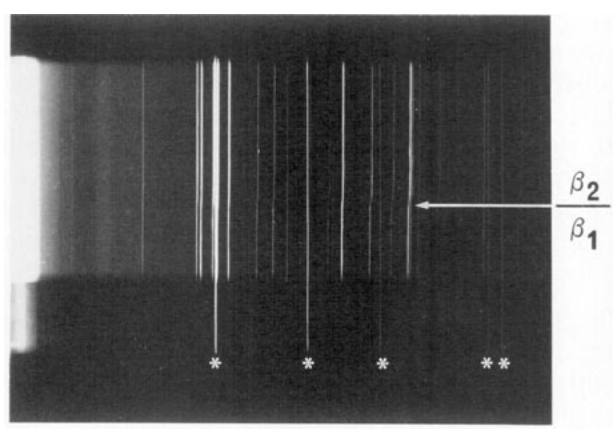

FIG. 4. Thermal evolution of the powder X-ray diffraction pattern (Guinier–Lenné camera, $\lambda = Cu K_\alpha$) of the $Bi_{0.75}Sr_{0.25}O_{1.375}$ phase (* = KCl lines).

change of the diffracted intensities, suggesting that the corresponding structural change is not very big.

This is confirmed by the values reported in Tables 1 and 2, and their evolution with temperature as illustrated in Figs. 5 and 6. They clearly indicate that the $\beta_2 \Leftrightarrow \beta_1$ transition corresponds to

- an increase of the delocalization of the "interstitial" anions, mainly by the creation of a new interstitial site O(3)′ at the expense of the O(2) site (see Figs. 5a and 7);
- an increase of the intersheet anionic population at the expense of the fluorite-like sheet anionic population, due to the migration of some interstitial anions from one side of the unsubstituted Bi-layers (M(2)-layers) to the other (see Figs. 5 and 7).

This small migration results in a high increase of the $(M(2)–M(2))_I$ distances, i.e., the Bi–Bi distances between Bi atoms of the external layers of two adjacent fluorite-like sheets, and therefore of the thickness d_I of the intersheet space (see Fig. 6).

3. *Structural Correlation with the Electrical Properties*

The thermal evolution of the electrical properties of the alkaline earth-doped rhombohedral phases and of their La-homologue are shown in Fig. 8. Three points are important:

(i) the conductivity is systematically higher for the La-doped phase than for the alkaline earth-doped ones, in both the β_1- and β_2-states;

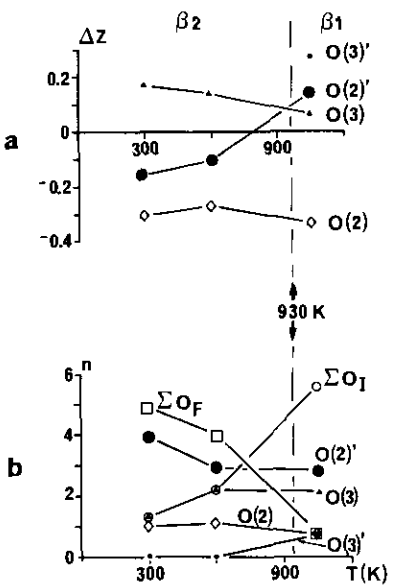

FIG. 5. Thermal evolution of (a) the position of "interstitial" anions with respect to the unsubstituted M(2) metal layers (positive Δz values correspond to anions within the intersheet space and negative Δz values correspond to anions within the fluorite-like sheets) and (b) the population of various anionic sites for the $Bi_{0.75}Sr_{0.25}O_{1.375}$ phase.

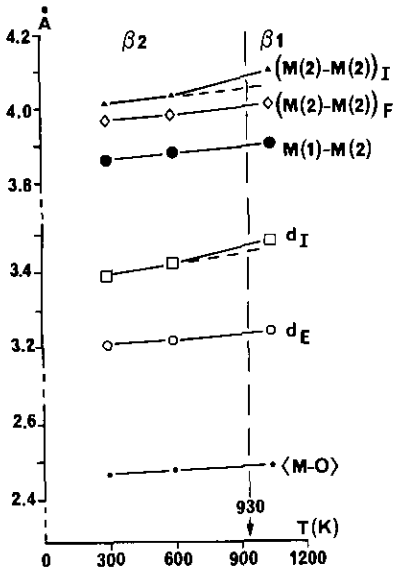

FIG. 6. Thermal evolution of the mean $\langle M–O\rangle$ distance of the main $M–M$ distances, and of the thicknesses d_F and d_I of respectively half the fluorite-like sheet and the intersheet space ($(M(2)–M(2))_F = M(1)–M(1) = a$).

(ii) the $\beta_2 \Leftrightarrow \beta_1$ transition results in a sudden increase of the conductivity, but the change is far more important for the alkaline earth-doped phases than for the La-doped homologues;

(iii) the conductivity in the β_1-state and the transition temperature decreases strongly in the order Ca > Sr > Ba for the alkaline earth-doped phases.

Each of these experimental facts can be explained on the basis of both the present and previous structural studies.

The bidimensional character of the diffusion process in these rhombohedral phases has been clearly demonstrated by the conductivity measurements of Conflant et al., (5, 14) performed on single crystals of the β_2-phase: the conductivity is two orders of magnitude lower parallel to the Oz-axis than perpendicular to it. We can exclude any contribution of the O(1) anions to the ionic conductivity since they are too tightly bound to the cationic network and their occupancy does not change when increasing the temperature. Therefore the migration process must correspond to the migration of O(2) anions via the interstitial O(2)′, O(3), O(3)′, and O(4) sites. Three pathways are possible. They are shown in Fig. 9, and the corresponding size of the diffusion windows and their evolution, with mean cation radius and with temperature, are illustrated in Figs. 10 and 11, respectively.

Pathway No. 1 is highly improbable for all phases because of the systematically lower size of the $F–F$ windows and of the very short $d_{W\text{-}O(1)}$ distances (see values in Table 2) that it implies.

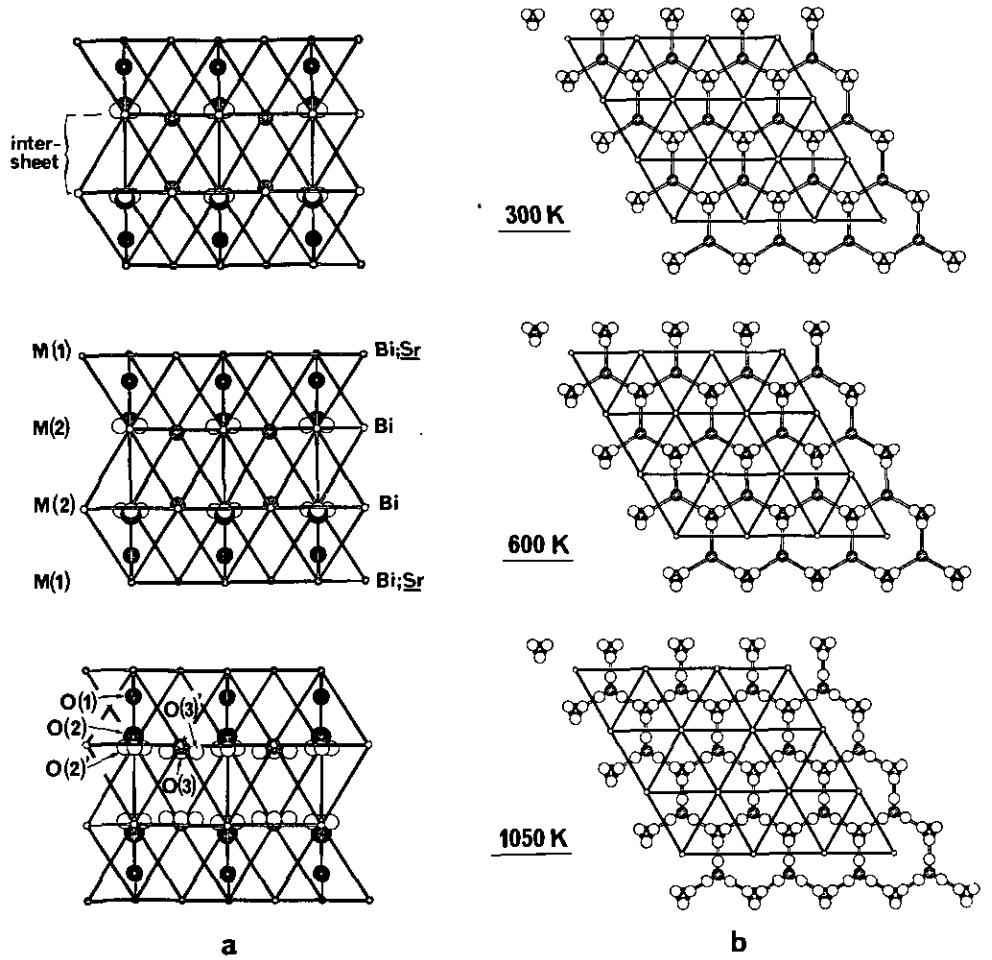

FIG. 7. Visualization of the thermal evolution of the anionic population in the vicinity of the unsubstituted $M(2)$ layers. View (a) along Oz and (b) normal to Oz.

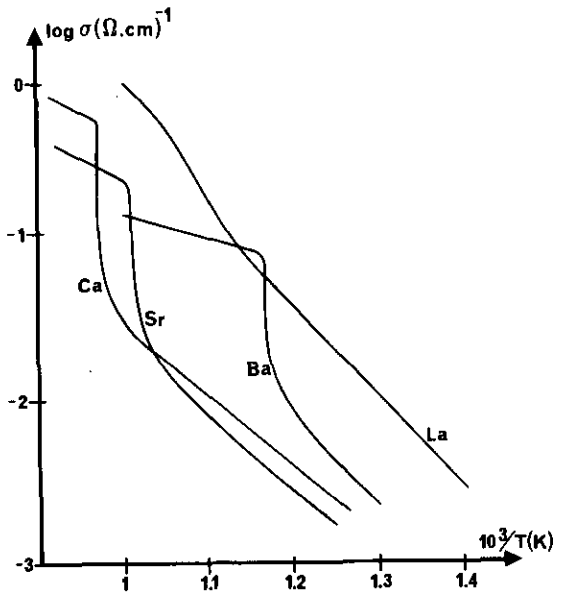

FIG. 8. Arrhenius plots for three alkaline earth-doped rhombohedral phases $Bi_{0.844}M_{0.156}O_{1.422}$ (M = Ca, Sr, Ba) and their $Bi_{0.850}La_{0.150}O_{1.50}$ homologue (10, 11).

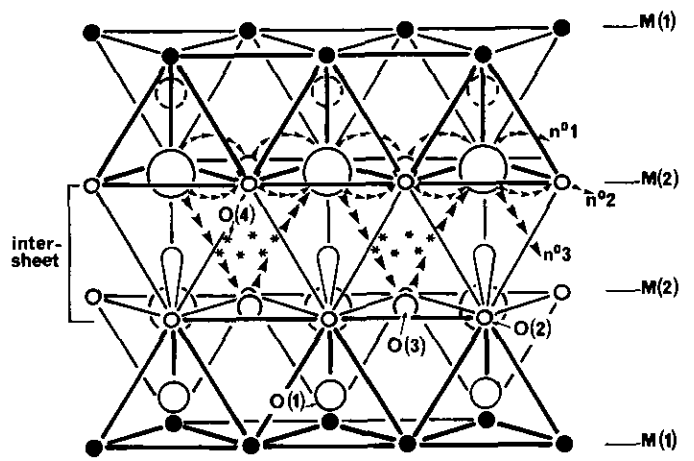

FIG. 9. Possible diffusion paths for anions in the alkaline earth- and La-doped rhombohedral phases.

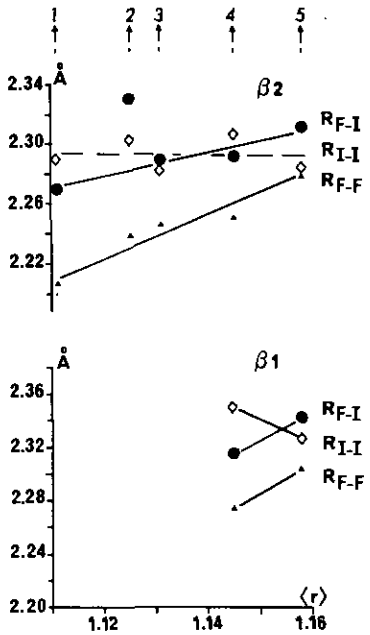

FIG. 10. Evolution with the mean cationic radius of the radius of the different windows that anions have to cross along the three possible paths. R_{F-F}, transversal window within the fluorite-like sheets; R_{I-I}, transversal window within the intersheet space; R_{F-I} = horizontal interface window. (1) $Ca_{0.156}Bi_{0.844}O_{1.422}$ (5); (2) $La_{0.30}Bi_{0.70}O_{1.50}$ (15); (3) $Sr_{0.56}Bi_{0.844}O_{1.422}$ (5); (4) $Sr_{0.25}Bi_{0.75}O_{1.375}$ (this work); (5) $Ba_{0.56}Bi_{0.44}O_{1.422}$ (5).

Pathways No. 2 and 3 are both possible for La and alkaline earth-doped phases. But it is highly probable that, due to (i) shorter d_1 distances (see Fig. 3) and (ii) higher sizes of the *I–I* and especially of the *F–I* windows (see Fig. 10), pathway No. 3 is followed only for La-doped phases. This is indicated by the exclusive presence of O(4) interstitial anions in these phases.

So, the increase of conductivity when substituting La for alkaline earths in rhombohedral phases would be the result of an increased mobility of the anions due to a lowering of potential barriers.

The sudden increase of the conductivity observed for alkaline earth-doped phases, at the $\beta_2 \rightarrow \beta_1$ transition, is a consequence of the migration of interstitial anions from the fluorite-like sheets to the intersheet space, which results in an increase of (i) the number of mobile anions and (ii) their mobility thanks to the increase in the size of the $F–I$ and overall the $I–I$ windows concerned (see Fig. 10).

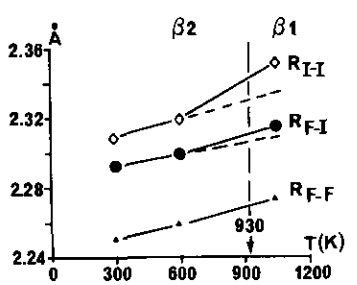

FIG. 11. Thermal evolution of the radius of the different windows for the $Bi_{0.75}Sr_{0.25}O_{1.375}$ phase.

The same migration probably occurs in the La-doped phases, but with a smaller influence on the window sizes, since they are already as large as in the β_1-state (see the abnormally high values of R_{I-I} and overall R_{F-I} in Fig. 10). This explains why the change in conductivity is not so abrupt in the case of the $Bi_{0.85}La_{0.15}O_{1.50}$ phase as in the alkaline earth-doped ones.

The decrease of the $\beta_2 \Leftrightarrow \beta_1$ transition temperature with increasing cation size (Ca > Sr > Ba) simply results from the important increase of the size of the windows in the *F–I* interface in the β_2-state and therefore of the ability for anions to migrate into the intersheet space. The decrease of the conductivity in the β_1-state results probably from the decrease in the size of the windows (see for example the high decrease from Sr- to Ba-doped phases of R_{F-I} and overall R_{I-I}).

V. CONCLUSIONS

Despite the relatively low accuracy of the high-temperature data (this study would have deserved to be completed by additional experiments on the D9 diffractometer at I.L.L. Unfortunately these experiments had to be postponed because of the reactor shutdown) our structural results have allowed us to understand the nature of the $\beta_2 \Leftrightarrow \beta_1$ phase transition observed in rhombohedral Bi_2O_3 doped with alkaline earth and rare earth oxides. This transition corresponds essentially to a migration of the delocalized interstitial anions from the fluorite-like sheets toward the intersheet space, which results in a steep increase of the number and mobility of charge carriers and therefore in a sudden increase of the conductivity.

REFERENCES

1. L. G. Sillen and B. Aurivillius, *Z. Kristallogr.* **101,** 483 (1939).
2. B. Aurivillius, *Ark. Kemi, Mineral. Geol.* **16A,** 1 (1943).
3. P. Conflant, J. C. Boivin, and D. Thomas, *J. Solid State Chem.* **18,** 133 (1976).
4. R. Guillermo, P. Conflant, J. C. Boivin, and D. Thomas, *Rev. Chim. Miner.* **14,** 153 (1978).
5. P. Conflant, Thèse de Doctorat ès Sciences, Université de Lille I, 1985.
6. T. Takahashi, T. Esaka, and A. Iwahara, *J. Appl. Electrochem.* **5,** 197 (1975).
7. H. Iwahara, T. Esaka, T. Sato, and T. Takahashi, *J. Solid State Chem.* **39,** 173 (1981).
8. D. Mercurio, M. El Farissi, B. Frit, J. M. Réau, and J. Sénégas, *Solid State Ionics* **39,** 297 (1990).
9. A. Aftati, Thèse, Universitè de Limoges, 1987.
10. P. Conflant, J. C. Boivin, G. Nowogrocki, and D. Thomas, *Solid State Ionics* **9,** 925 (1983).

11. T. Takahashi, H. Iwahara, and Y. Nagai, *J. Appl. Electrochem.* **2,** 97 (1972).
12. P. Demonchy, P. Conflant, J. C. Boivin, and D. Thomas, *C. R. Acad. Sci.* **289,** 317 (1979).
13. J. C. Boivin and D. Thomas, *Solid State Ionics* **3,** 457 (1981).
14. P. Conflant, J. C. Boivin, and D. Thomas, *J. Solid State Chem.* **35,** 192 (1980).
15. S. K. Blower and C. Greaves, *Mater. Res. Bull.* **23,** 765 (1988).
16. D. Mercurio, M. El Farissi, J. C. Champarnaud-Mesjard, B. Frit, P. Conflant, and G. Roult, *J. Solid State Chem.* **80,** 133 (1989).
17. M. Thomas, R. F. Stansfield, M. Berneron, A. Filhol, G. Greenwood, J. Jacobe, D. Feltin, and S. A. Mason, *in* "Position Sensitive Detection of Thermal Neutrons" (P. Convert and J. B. Forsyth, Eds.), p. 344. Academic Press, London, 1983.
18. C. Wilkinson and H. W. Khamis, *in* "Position Sensitive Detection of Thermal Neutrons" "P. Convert and J. B. Forsyth, Eds.), p. 359. Academic Press, London, 1983.
19. G. M. Sheldrick, "SHELX 76: A Program for Crystal Structure Determination." University of Cambridge, Cambridge 1976.
20. R. D. Shannon and C. T. Prewitt, *Acta Crystallogr. Sect. B* **25,** 925 (1969).